RSC Advances

ROYAL SOCIETY OF CHEMISTRY

www.rsc.org/advances

RSC Advances

PAPER

Preparation and characterization of a novel porous Ti/SnO_2-Sb_2O_3-CNT/PbO_2 electrode for anodic oxidation of phenol wastewater

Received 00th January 20xx,
Accepted 00th January 20xx

DOI: 10.1039/x0xx00000x

www.rsc.org/

Juntao Xing,[a] Donghui Chen, [a] Wei Zhao, *[ab] Xiuxian Zhao[a] and Wenwen Zhang[a]

Porous Ti/SnO_2-Sb_2O_3-CNT/PbO_2 electrodes were successfully fabricated using thermal decomposition technique and electro-deposition technologies. Characterization experiments including Scanning electron microscopy (SEM), Energy-dispersive spectroscopy (EDS), X-ray diffraction (XRD), Cyclic voltammertry (CV), Electrochemical Impedance Spectroscopy (EIS) and accelerated life time test was performed to evaluate the effect of CNT-doped SnO_2-Sb_2O_3 intermediate layer on PbO_2 electrode. The results showed that CNT could be doped into the SnO_2-Sb_2O_3 intermediate layer by thermal decomposition. Compared with porous Ti/SnO_2-Sb_2O_3 substrate, CNT-doped induced the substrate surface forming a fibrous structure, it means that porous Ti/SnO_2-Sb_2O_3-CNT substrate would provide more active sites for PbO_2 deposition and could make a compact and fine surface coating. Besides, the CNT modified electrode had higher active surface area and higher electrochemical activity than without CNT doped. The life of porous Ti/SnO_2-Sb_2O_3-CNT/PbO_2 (296h) was 1.38 times as much as that of porous Ti/SnO_2-Sb_2O_3/PbO_2 electrode (214h). Electro-catalytic oxidation of phenol in aqueous solution was studied to evaluate the electrochemical oxidation ability in environment science. Porous Ti/SnO_2-Sb_2O_3-CNT/PbO_2 electrode displayed not only excellent electro-catalytic performance but also low energy consumption using phenol as a model organic pollutant. The porous Ti/SnO_2-Sb_2O_3-CNT/PbO_2 electrode has higher kinetic rate constant and chemical oxygen demand (COD), which is 1.73 and 1.09 times those of the porous Ti/SnO_2-Sb_2O_3/PbO_2 electrode, respectively. Moreover, CNT-doped can further increase the hydroxyl radical (·OH) generation capacity. All these results illustrated that porous Ti/SnO_2-Sb_2O_3-CNT/PbO_2 electrode for pollutants degradation and had a great potential application.

1. Introduction

In recent years, electrochemical oxidation of aqueous wastes containing non-biodegradable organics such as phenol[1], lignin[2], 4-chlorophenol[3], pentachlorophenol[4], perfluorocarboxylic acids[5], has been extensively studied, which attributed to its many distinctive advantages[6] including environmental compatibility, versatility energy efficiency, low-volume application, and amenability to automation[6-8]. For electrochemical oxidation, it is learnt that anode material plays a critical role on the organic pollutants degradation[9]. The reason is that electrode materials are conclusive for optimizing electrochemical oxidation process because of their impacts on the effectiveness of mechanisms and reaction pathways[10]. Hence, the research hotspot mainly focused on the development of stable anodes for removal of persistent organic pollutants by electrochemical oxidation[7, 11].

To date, literature results summarized showed that there are two main research focus of electrochemical oxidation. The first research focus is to explore novel anode materials. The nature of electrode material strongly affects both process selectivity and efficiency. In particular, anodes with low oxygen evolution overpotential, such as graphite[12], RuO_2[13], and Pt[14] permit only partial oxidation of organics, while anodes with high oxygen evolution overpotential, such as SnO_2[15], PbO_2[16], and BDD[17], favor high potential for anodic oxidation of organic compounds. Among them, BDD anodes show the highest removal rate and stability, but, its high cost and especially the difficulties to find an appropriate substrate for deposition of the diamond layer limit its large-scale application. The second research focus is to dope some metal elements into oxide layer or the intermediate layer which can enhance the electro-catalytic activity and chemical or mechanical stability of oxide electrodes[18, 19], such as, doping with rare earth (Ce, Pr, La, etc.)[20-23] and some metal (Au, Fe, Bi, etc.)[24-26]. Although the above methods show high effective for electro-catalytic oxidation of organic pollution, some problems still restrict its practical application, such as short service life, complex preparation process and so on.

In order to enhance more reaction active sites and more contacts between coating catalyst and reactant to promote electro-catalytic efficiency, we introduced porous Ti substrate and carbon nanotubes (CNTs) into SnO_2-Sb_2O_3 intermediate layer to prepare a novel porous Ti/SnO_2-Sb_2O_3-CNT/PbO_2 electrode. As a novel titanium matrix, porous Ti has the advantages of good corrosion resistance, high porosity, large surface area and good biocompatibility, widely used in aerospace, medical and chemical field[27, 28]. Recent studies

[a] School of Chemical and Environmental Engineering, Shanghai Institute of Technology, Shanghai 201418, China. E-mail: chendhsit@163.com; Tel: +86 13817007038
[b] College of Environmental Science and Engineering, Donghua University, Shanghai 201620, China.

reveal the significance of porous Ti on improving the performance of electrodes. Zhao *et al.* focused on systematically studying the effect of a porous Ti substrate on the surface structure and electrochemical properties of lead dioxide electrodes[28]. Zhang *et al*. found that the PbO_2/AC asymmetric electrochemical capacitor (AEC) based on porous-Ti/PbO_2 has high energy density over traditional electrochemical capacitors and long lifespan over traditional lead acid batteries[29]. In addition, carbon nanotube (CNT) is a novel material with good electrical properties and high chemical stability discovered by Iijima in 1991.[30] CNTs have been proposed as the ideal metal catalyst support for sensing and electro-catalytic application.[15, 31-33] The literatures mainly focused on that CNT has been doped into the oxide layer to improve the catalytic ability of electrode by electro-deposition method[34], but, little attention has been paid to CNT doped into the intermediate layer of electrode by other methods. It is also expected that the CNT-doped can not only improve the catalytic performance of electrode, but also can increase the specific surface area and enhance more contacts to increase electrodes service life.

In this paper, we propose a novel modification method for PbO_2 electrode with the aim of improving the performance of PbO_2 electrode. To the best of our knowledge, CNT is first introduced into SnO_2-Sb_2O_3 intermediate layer by thermally deposited. In addition, a systematic study was carried out to investigate the preparation and characterization of porous Ti/SnO_2-Sb_2O_3-CNT/PbO_2 compared with porous Ti/SnO_2-Sb_2O_3 /PbO_2 without CNT-doped. The modified electrode was characterized, including morphology, crystalline structure, electrochemical performance and the accelerated service life. The oxidation performance and utilization of hydroxyl radicals on the electrodes was also evaluated. Phenol, as one of the widely used pollutant in industrial wastewater, was selected as the target pollutant.

2. Experimental

2.1.Materials

The CNT was purchased from Chengdu Organic Chemicals Co., ltd. (China) with an outer diameter of 50nm, and length of 10-20μm. Porous Titanium (purity 99.9%, 20mm×10mm×1mm) was purchased from Baoji Jinkai Industrial Technology Co., Ltd. All the chemicals used in the experiments were received without further purification. All solutions used in this work were prepared with deionized water.

2.2. Electrode preparation

2.2.1 Titanium surface treatment. In order to prepare for a good adhesive metal oxide film material, porous titanium substrate were pretreated according the following procedure. First, a porous titanium (20 mm×20 mm×1 mm) was mechanically polished with 600-grid abrasive papers. Then, the porous titanium substrate was cleansed with deionized water and acetone to remove solid particles and grease. Second, it was subsequently immersed in sodium hydroxide (15% m/m) at the temperature of 60℃ for 30min and then was etched in boiling hydrochloric acid (30% v/v) about 60 min to produce a gray surface with uniform roughness. Finally, it was washed by ultrasonic cleaning in ultrapure water and stored in deionized water.

2.2.2 Coating SnO_2-Sb_2O_3-CNT. The SnO_2-Sb_2O_3-CNT intermediate layer was prepared on porous titanium substrates by thermal decomposition. The coating solution was prepared by firstly dissolving 1mL concentrated HCL in 25 ml isopropanol and then raising the solution temperature to 80 ℃ for dissolving 6.65 g $SnCl_4.5H_2O$、0.475 g $SbCl_3$、0.1 g CNT.

The treated titanium substrate was dipped in the solution for 5min, and then dried at about 130 ℃ for 10 min with excess solvent being evaporated by hot air. then the treated titanium substrate was calcined at 500 ℃ for 15 min in muffle furnace. All the above processes were repeated twelve times. For the last time, the electrodes were annealed at 500 ℃ for 60 min.

2.2.3 Electrochemical deposition PbO_2. PbO_2 was deposited onto Ti/SnO_2-Sb_2O_3-CNT (geometric area:1.0×1.0 cm^2) under the current density of 20 mA·cm^{-2} at 65℃for 1 h with magnetic stirring. The coating solution consisted of 0.1 M HNO_3 acidic media containing 0.5 M $Pb(NO_3)_2$ and 0.04 M NaF. After electro-deposition, the modified electrode was rinsed with deionized water. Porous Ti/SnO_2-Sb_2O_3/PbO_2 electrode without CNT doped was made by the above same method. In the electro-deposition system the copper foil electrode (20 mm × 20 mm) was used as cathode.

More details concerning electrode preparation are given in our previous study[35].

2.3. Electrode characterization

2.3.1 Physicochemical Characterization. A Japan RigaKu D/MAX2200PC diffractometer with Cu-Kα radiation (0.15418 nm) incident radiation was employed to analysis the Crystal structure of electrodes. Surface morphologies of different electrodes were characterized by a HITACHI S-3400N scanning electron microscope. For the elemental analysis and spectral mapping, a Thermo Noran EDS spectrometer equipped with SYSTEM SIX was used.

2.3.2 Electrochemical measurement. Cyclic voltammetry (CV) was executed in the CHI760D electrochemical workstation (Chenhua Instrument Shanghai Co., Ltd, China) with conventional three-electrode cell. The fabricated PbO_2 electrodes were used as working electrode, a saturated calomel electrode (SCE) as the reference electrode and a platinum sheet electrode as the counter electrode. Anti-corrosion performance of the electrodes was investigated using accelerate lifetime test with a current density of 500 mA cm^{-2} in 3.0 mol L^{-1} H_2SO_4 solution was recorded simultaneously. The service life of the electrodes was considered to be terminated when the cell voltage reaches up to 10 V.

All electrochemical experiments were carried out at room temperature (25 ± 2 ℃). All solutions were prepared with deionized water and all reagents used in the experiments were analytic grade.

2.4. Electrochemical degradation tests

Phenol was selected as the sample of aromatic contamination for studying the CNT modified electrodes. The electrochemical degradation was carried out in a cylindrical single compartment cell equipped with a magnetic stirrer and a jacketed cooler to maintain a constant temperature. The fabricated PbO_2 electrode was used as anode and the stainless copper with the same dimension was used as cathode with a distance of 1.5 cm between the two electrodes.

The current density was controlled to be constant 30 mA cm^{-2} by a direct current power supply (RXN-605D, China). The stirring rate was about 800 rpm. The experiments were carried out at 25℃ for 300 min. The volume of phenol solution was 80mL with an initial concentration of 100mg L^{-1} and 0.1mol L^{-1} Na_2SO_4 was added to the solution. During the experiments, liquid samples were withdrawn from the electrolytic cell at the fixed time interval to determine the variation of phenol concentration, COD and evaluate reaction kinetics. The concentration of phenol was analyzed using a Varian high performance liquid-chromatography (HPLC) with a UV detector set at 270 nm. A C-18 column was used to separate the organics while the mobile phase made of 30% CH_3CN and 70% water was at a flow rate of 1 mL/min. COD was digested by potassium dichromate using a 5B-1F Speed Digester (Lianhua Tech Co., China) at 150 C for 10 min and determined by ultraviolet spectrophotometry at 610 nm using a TU-1810 Uv/visible analysis spectrophotometer (Beijing Puxi Instrument Co. Ltd.). Each experiment was conducted for three times, in order to keep the relative standard deviations (RSD) less than 5%.

The General current efficiency (GCE), representing an average value of current efficiency, between the initial time *t = 0* and *t*. It was calculated based on the results of COD test and the following equation[7]:

$$GCE = \frac{(COD_0 - COD_t)}{8It} \mathrm{FV}$$

Where COD_0 and COD_t are the experimental values of phenol at times *t = 0* (initial) and *t* (mg/L), respectively; *I* is the electrolysis current (A), *F* is Faraday's constant (96 485C/mol) and *V* is the volume of the solution (L), and 8 is the oxygen equivalent mass (g/eq).

The specific energy consumption (SEC) was the energy consumption for the removal of one kg of COD and calculated as follows (express in kWh)[8]:

$$SCE = \frac{IUt}{(COD_0 - COD_t)\mathrm{V}}$$

Where *t* is the electrolysis time (h), *U* and *I* are the average cell potential (V) and current (A), V is the sample volume (L), COD_0 and COD_t are the difference in COD (mg/L).

In addition, we used the fluorescence method based on terephthalic acid, which is a well-known ·OH scavenger that can be used for estimating the amount of ·OH radicals generated under various conditions by a fluorescence spectrophotometer (Perkin-Elmer LS-50, American). An aqueous solution of a 200 mL volume containing 0.5 mol L^{-1} terephthalic acid, 0.5 g L^{-1} NaOH and 0.25 mol L^{-1} Na_2SO_4 was used as the electrolyte solution. The anode was a prepared PbO_2 electrode and the cathode was a stainless steel sheet. Hydroxyl radical production was performed at a current density of 30 mA cm^{-2} at 30 ℃. During the experiments, samples were drawn from the reactor every 5 min and diluted 10 times with deionized water, then analyzed with a fluorescence spectrophotometer. The fluorescence spectra were recorded in the range of 380 to 520 nm, using a 315 nm excitation wavelength.

3. Results and discussion

3.1. Surface morphology and crystal structure

3.1.1.Morphological analysis and film composition. The SEM cross section morphology of different electrodes was shown in Fig.1(a-d). It can be clearly seen that the surface or internal of porous titanium substrate was very rough and had irregular pores with average sizes of 30 um which can provide a larger specific surface area than the traditional plate titanium substrate. In addition, The results of EDS in Fig.1(e-f) showed that SnO_2-Sb_2O_3 Intermediate layer and CNT can be distributed into the internal of porous titanium by thermal decomposition (Pt peak comes from the platinum coating for SEM). However, CNT-Doped SnO_2-Sb_2O_3 films does not reveal major changes compared to undoped electrode through the SEM cross section morphology .

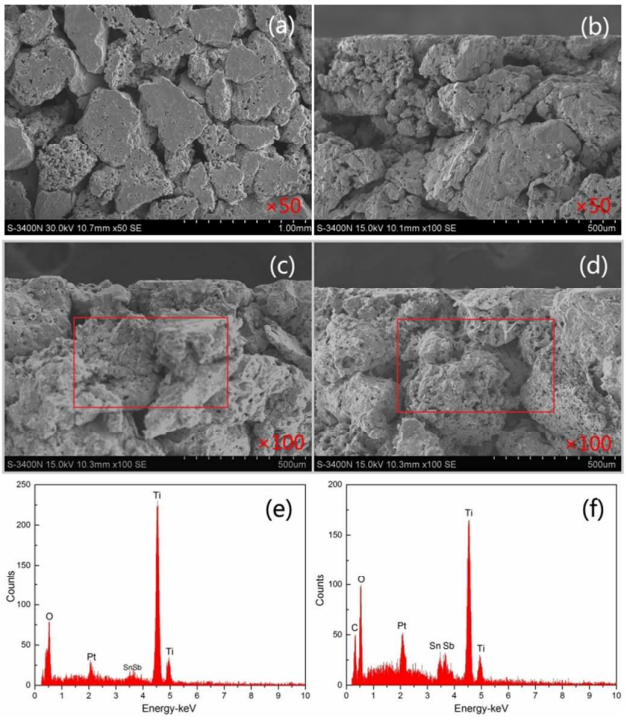

Fig.1 SEM micrograph of (a) porous Ti substrate surface (×50), cross-sections for (b) Porous Ti substrate (×100), (c) Porous Ti/SnO_2-Sb_2O_3 electrode(×100), (d) Porous Ti/SnO_2-Sb_2O_3–CNT electrode(×100), (e) EDS of the zone in (c), (f) EDS of the zone in (d).

Fig.2 (a-d) shows the morphologies of the interlayer and surface layer of different electrodes. It is clearly seen from Fig.2(a-b) that the introduction of CNT doped into SnO_2-Sb_2O_3 interlayer film significantly affected the film morphology. In contrast with porous Ti/SnO_2-Sb_2O_3 substrate, CNT-doped induced the substrate surface forming a fibrous structure, hence porous Ti/SnO_2-Sb_2O_3-CNT had larger specific surface area, which could provide with more active sites for electro-catalytic oxidation. Besides, the fibrous structure can make the PbO_2 deposited more firmly and tightly. The CNT-modified electrode was expected to have better electrochemical properties and physic-chemical properties, which was further proved by the following experiments. To further check the impact of CNT-doped on the formation of PbO_2, Fig.2(c) and 2(d) displays the electrode crystal structure and appearance of porous Ti/SnO_2-Sb_2O_3/PbO_2 and porous Ti/SnO_2-Sb_2O_3-CNT/PbO_2 with a

magnification of 100×, 4000× in the insets, respectively. It is noticeable that particles sizes of porous Ti/SnO_2-Sb_2O_3-CNT/PbO_2 become smaller than that of porous Ti/SnO_2-Sb_2O_3/PbO_2, the coating particles grown on the SnO_2-Sb_2O_3-CNT intermediate layer did not present fissures or laminations and appeared to be more compact and uniformly distributed.

Fig.2(g) and Fig.2(h) show the EDS spectrum of the coating of porous Ti/SnO_2-Sb_2O_3 and porous Ti/SnO_2-Sb_2O_3-CNT respectively (Pt peak comes from the platinum coating for SEM). The Sn, Sb, Ti and O were clearly all observed, indicating the formation of the oxide mixture of Sn and Sb. Due to porous Ti with larger surface areas, so the oxide layer may not completely cover porous Ti substrate surface. The C peak was detected in EDS (Fig.2(h)), showing that CNT was successfully doped into the middle layer (SnO_2-Sb_2O_3) by thermal decomposition method and not oxidized during the calcination process. This result was not consistent with the result reported in literature[15]. Based on the results from the SEM and EDS analyses, we conclude that the CNT was successfully doped into SnO_2-Sb_2O_3 intermediate layer by calcinations process and would be beneficial to electrochemical properties. Based on the results from the above SEM-EDS analyses, the formation process of porous Ti/SnO_2-Sb_2O_3-CNT is described in Fig.3. In addition, we use the gravimetric method to calculate the growing rate of SnO_2-Sb_2O_3-CNT/PbO_2 and the value is 1.979mg/cm^2.

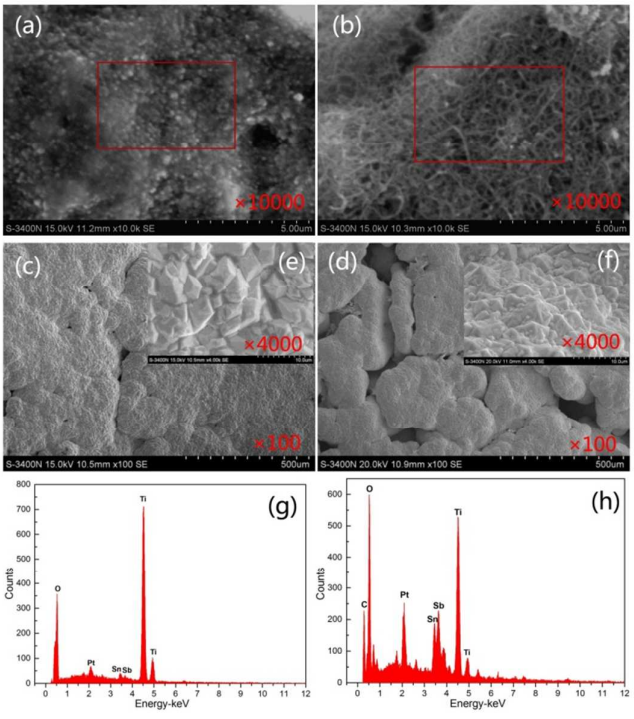

Fig.2 SEM micrograph of electrodes. (a) Porous Ti/SnO_2-Sb_2O_3 electrode (×10000), (b) Porous Ti/SnO_2-Sb_2O_3–CNT electrode (×10000), (c) Porous Ti/SnO_2-Sb_2O_3/PbO_2 electrode (×100), (d) Porous Ti/SnO_2-Sb_2O_3-CNT/PbO_2 electrode (×100), insets in (c) and (d) are SEM images with high magnification (×4000) corresponding to the electrode. (g) EDS of the zone in (a), (h) EDS of the zone in (b).

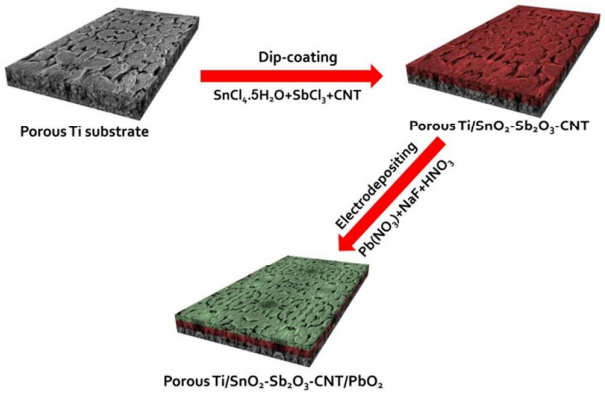

Fig.3 Schematic illustration for the fabrication of Porous Ti/SnO_2-Sb_2O_3–CNT/PbO_2 electrode.

3.1.2.Structural analysis by XRD. The crystal structure of the PbO_2 coating deposited on porous Ti/SnO_2-Sb_2O_3-CNT substrate was determined by X-ray diffraction. The corresponding patterns of the PbO_2 coatings with different substrate is shown in Fig.4. It can be seen that the XRD of PbO_2 coatings based on different substrates are quite similar, but the reflection intensities of CNT-doped coating increased and the half-widths of the reflection peaks decreased, meaning that the degree of crystallization were increased and the crystallite size decreased owning to CNT-modified. In addition, Fig.4 displays the main diffraction peaks at 2θ=25.4°, 32.0°, 36.2°, 49.2°, 52.1°, 59.2°, 62.3°, 74.4°, 84.3° and 85.9° which are assigned to the (110), (101), (200), (211), (220), (310), (301), (321) ,(312)and (411) planes of β-PbO_2, and the strong main crystal plane of β-PbO_2 is (101), (211) and (301) plane. At the same time, some weak peaks (2θ=67.8°, 76.9°) infer the presence of a-PbO_2. However, no diffraction peaks of tin and antimony oxides are observed, indicating that the active layer of PbO_2 was uniform and thus tin and antimony oxides were undetected by XRD. This was also confirmed by the above SEM results.

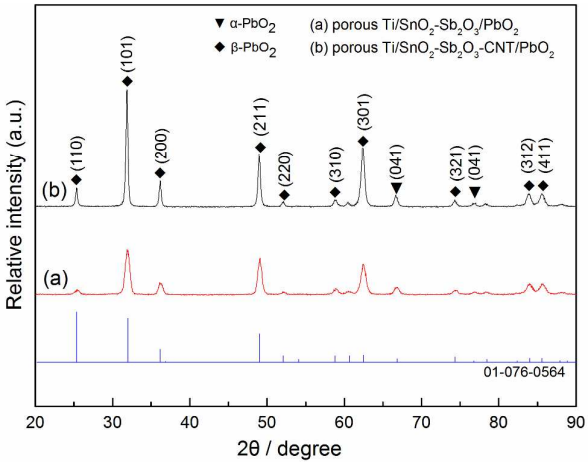

Fig.4 XRD patterns of (a) porous Ti/SnO_2-Sb_2O_3/PbO_2 electrode, (b) porous Ti/SnO_2-Sb_2O_3-CNT/PbO_2 electrode.

3.2 Electrochemical characterization of electrode

3.2.1 Electrochemical active surface area. Electrochemical active surface area means that the active sites are accessible to electrolyte when electrochemical reaction occurs. The voltammetric charge quantity (*q**), which is related to real surface area and the number of active sites, can reflect the electrochemical activity of an electrode. Larger *q** indicates higher electrode activity. We employed the method reported in literature[36-38] to calculated *q** for estimating the electrode activity. The equation can be expressed as follows:

$$(q^*)^{-1} = (q_T^*)^{-1} + kv^{1/2} \quad (1)$$

The total charge quantity q_T^* stands for the quantity of theoretically electrochemical active sites of electrode surface, and v stands for the scan rate of voltage, while *k* is a constant. In order to determine the electrochemical active surface areas of porous Ti/SnO_2-Sb_2O_3/PbO_2 and porous Ti/SnO_2-Sb_2O_3-CNT/PbO_2, *q** was tested in Na_2SO_4 solution. Special adsorption occurs between sulfate ion and PbO_2 forming insoluble $PbSO_4$, which results in pseudo-capacitance (Eq.(2) and (3)):

$$H^+ + SO_{4ads}^{2-} \Leftrightarrow HSO_{4ads}^- \quad (2)$$

$$4HSO_{4ads}^- + PbO_2 + 2e^- = PbSO_{4ads} + 3SO_{4ada}^{2-} + H_2O \quad (3)$$

So the q* in the pseudo-capacitance region of PbO2 in Na2SO4 solution can be defined as the electrochemical active surface area of PbO2 in sulfate electrolyte. Fig.5A shows the cyclic voltammograms of porous Ti/SnO_2-Sb_2O_3/PbO_2 and porous Ti/SnO_2-Sb_2O_3-CNT/PbO_2, q* was integrated from cycle voltammetric curves over the whole potential range from 0.3 V to 0.8 V. The relationship of the reciprocal of q* versus square root of scan rate is shown in Fig.5B. For PbO2 electrodes, the q* at low scan rate reflects the deep discharge performance; the *q** at high scan rate reflects the power performance. The *q** of PbO_2 electrode at scan rate of 10 and 50 mV s^{-1} are listed in Table 1. *k* constant is the slope off our straight lines in Fig.5B. *k* constant represents the change rate of electrochemical active surface area with increasing scan rate. The smaller *k* constant is, the slower the electrochemical active surface area declines with increasing the scan rate. Therefore, comparing with the value of *q** and *k*, the result indicated that the porous Ti/SnO_2-Sb_2O_3-CNT/PbO_2 electrode had the highest active surface area.

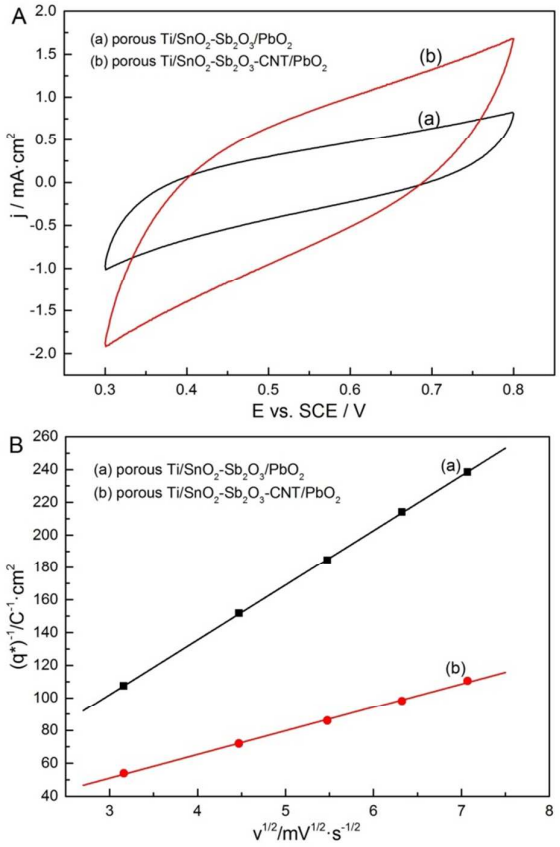

Fig.5 (A) Cyclic voltammograms of (a) porous Ti/SnO_2-Sb_2O_3/PbO_2, (b) porous Ti/SnO_2-Sb_2O_3-CNT/PbO_2 electrode in 0.5 mol L^{-1} Na_2SO_4 solution at scan rate of 50 mV s^{-1}. (B) Relationship of the reciprocal of voltammetric charge quantity versus square root of scan rate: (a) porous Ti/SnO_2-Sb_2O_3/PbO_2, (b) porous Ti/SnO_2-Sb_2O_3-CNT/PbO_2 electrode.

Table 1 Voltammetric charge information of different electrodes.

Electrode	k constant	q* at 10 mV.s^{-1}	q* at 50mV.s^{-1}
porous Ti/SnO_2-Sb_2O_3/PbO_2	33.5588	0.0093	0.0042
porous Ti/SnO_2-Sb_2O_3-CNT/PbO_2	14.3733	0.0186	0.0091

3.2.2 Cyclic voltammetry. Fig.6 shows the cyclic votammograms of different electrodes in the potential range between 0.8 V and 2.0 V in 0.5 mol L^{-1} H_2SO_4 solution. As can be observed, the oxidation-reduction properties of electrodes appear to be more or less similar. The oxidation peak appeared in the anodic branch of the curve, which indicated that Pb^{2+} ($PbSO_4$) could be oxidized Pb^{4+} (PbO_2) between 1.7 and 1.8 V (vs.SCE). In the cathodic branch curve, a reduction peak might be attributed to the generation of Pb^{2+} ($PbSO_4$) from the following reaction[39 29] between 1.0 and 1.2 V (vs.SCE).

$$PbO_2 + H_2SO_4 + 2H^+ + 2e^- \Leftrightarrow PbSO_4 + 2H_2O \quad (4)$$

In addition, The CNT-modified electrode presented higher oxidation-reduction peak currents than other electrode without CNT-doped, meaning that many more substances involved in oxidation reaction. The reason mainly lies in that porous Ti/SnO_2-Sb_2O_3-CNT/PbO_2 electrode has larger active surface areas which provide more active site for electrochemical reaction. The result also further proved by the above conclusion. In conclusion, the introduction of CNT-doped interlayer is expected to increase the oxidation ability and catalytic activity of porous Ti/SnO_2-Sb_2O_3/PbO_2.

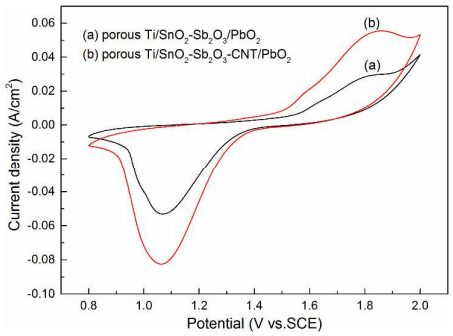

Fig.6 Cyclic voltammograms curves of different electrodes (a) porous Ti/SnO_2-Sb_2O_3/PbO_2, (b) porous Ti/SnO_2-Sb_2O_3-CNT/PbO_2 in 0.5 mol L^{-1} H_2SO_4 solution at scan rate of 50 mV s^{-1}.

3.2.3 Electrochemical impedance. EIS is a powerful technique to study porous electrode. To understand the effect of the CNT-doped, we did further EIS studies. Fig.7 presents electrochemical impedance of porous Ti/ SnO_2-Sb_2O_3/ PbO_2 (a) and porous Ti/SnO_2-Sb_2O_3-CNT/PbO_2 electrode (b) in 0.5 mol/L H_2SO_4 solution at oxygen evolution region (1.8 V vs SCE). The equivalent circuit shown in Fig.8 was used to fit the EIS data. The simulated data of each parameter in Fig.7 is listed in Table 2. In this $R_s(R_{ct}Q_{dl})$ circuit, R_s represents ohmic resistance including the resistance of electrolyte and active material. R_{ct} stands for charge-transfer resistance, reflecting oxygen evolution reaction activity. Q_{dl} is introdued to replace the electric double layer capacitor.

Two obvious semicircles appeared in electrochemical impedance spectra from Fig.7. The diameter of the semicircle size reflects R_{ct} and the resistance values were 1.315 Ω·cm^2 and1.187 Ω·cm^2 in Table 2 respectively, indicating that the oxygen evolution reaction activity of porous Ti/SnO_2-Sb_2O_3-CNT/PbO_2 electrode was slightly higher. According to the reaction mechanism of electrode oxygen evolution, the oxygen evolution activity depends on the active sites of active coating, the more the active sites, the greater the reaction activity. Hence CNT-doped into Intermediate layer also increases the active sites which can provide larger specific surface area. The result was also further proved by R_s values in Table 2 that porous Ti/SnO_2-Sb_2O_3-CNT/PbO_2 electrode prepared had the smallest R_s, indicating the largest electrochemical active surface area. From the above results, it can conclude that CNT doped can reduce the resistance of active material.

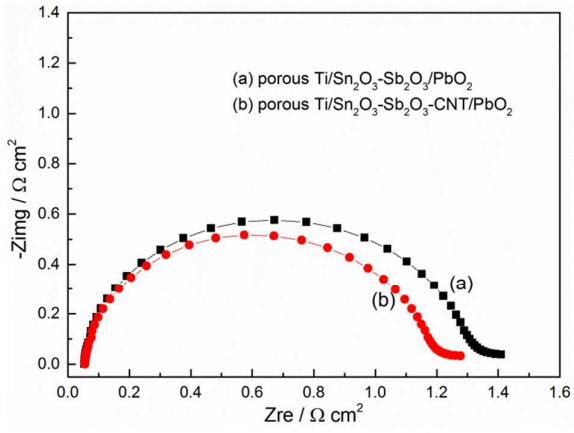

Fig.7 EIS plots in the 0.5 M acidic solution: (a) porous Ti/SnO_2-Sb_2O_3/PbO_2,(b)porous Ti/SnO_2-Sb_2O_3-CNT/PbO_2 electrode. Electrode potential: 1.8 V vs SCE.

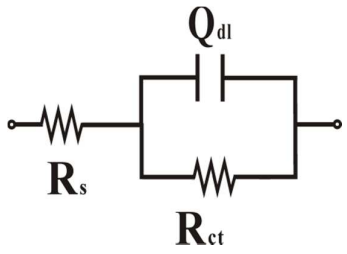

Fig.8 Equivalent circuit used in the analysis of the experimental EIS data.

Table 2 Simulated values of each electrical element.

Electrode	R_s/Ω cm^2	Q_{dl}/Ω $cm^{-2}s^n$	R_{ct}Ω/Ω cm^2	n
porous Ti/ SnO_2-Sb_2O_3/PbO_2	0.3962	0.0067	1.315	0.9591
porous Ti/ SnO_2-Sb_2O_3-CNT/PbO_2	0.2847	0.0079	1.187	0.9531

3.2.4 Electrode stability. The service life is another important factor to be considered for the electrode quality and practical application. As shown in Fig.9, the service life of porous Ti/SnO_2-Sb_2O_3-CNT /PbO_2 was 291 h, as much as 1.35 times that of porous Ti/SnO_2-Sb_2O_3/PbO_2 (214 h). The results reveal that doping the CNT into SnO_2-Sb_2O_3 interlayer film can improve the electrochemical stability. The improved service lifetime can be attributed to the following reasons. Firstly, it resulted from the decrease of the PbO_2 particle size which can make a compact and fine surface layer as observed from the SEM images in Fig.2. The compact surface can baffle the penetration of the supporting electrolyte toward the titanium substrate through the cracks and delay the formation of non-conductive TiO_2 layer. Secondly, the fibrous structure of SnO_2-Sb_2O_3-CNT interlayer itself can make PbO_2 deposited more tightly and reduced the film detachment.

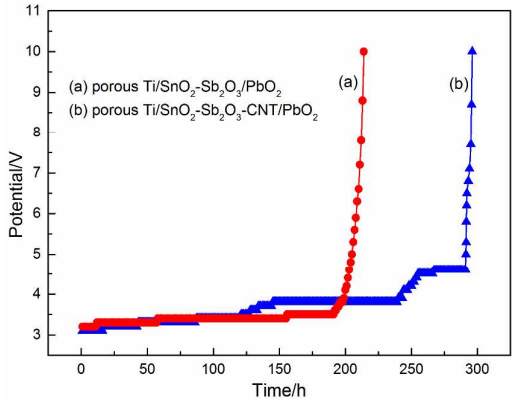

Fig.9 Accelerated life test of (a) porous Ti/SnO_2-Sb_2O_3/PbO_2 electrode and (b) porous Ti/SnO_2-Sb_2O_3-CNT/PbO_2 electrode in 3 mol L^{-1} H_2SO_4 solution under 0.5 A cm^{-2}.

3.3 Electrochemical degradation test

3.3.1. Electrochemical degradation of phenol. To further investigate the influence of CNT-doped on the electro-catalytic degradation activity of electrode, degradation experiments were

carried on different electrode. The variations of removal efficiency for phenol with electrolysis time are shown in Fig.10. It can be clearly seen that the removal efficiency rates are up to 94% within 300 min for porous Ti/SnO_2-Sb_2O_3-CNT/PbO_2 electrode, only 80% for porous Ti/SnO_2-Sb_2O_3/PbO_2 electrode. So the modified electrode with CNT-doped significantly improved the phenol removal performance.

In addition, the processes of degradation were found well fit pseudo-first-order model for all electrodes as Eq.(5). And the fitting results were shown in Fig.10B.

$$\ln\left(C_0/C\right) = -kt \qquad (5)$$

Where C_0 is the initial concentration of phenol, C is the concentration of phenol at given time t. and k is the kinetic rate constant[40]. The k values for the two electrodes were 0.0088 min^{-1} and 0.0051 min^{-1}. The reaction rate constant of porous Ti/SnO_2-Sb_2O_3-CNT/PbO_2 electrode was 1.73 times greater than that of porous Ti/SnO_2-Sb_2O_3/PbO_2. That suggested that phenol could be degraded more rapidly on the CNT-doped electrode.

The COD reduction is very important to monitor the performance of the different electrodes. Hence, COD removals of phenol by the two different electrodes were compared to further evaluate the effect of the CNT doped for the electro-catalytic oxidation. The variation of COD with electrolysis time was shown in Fig10. Clearly, the COD was removed more rapidly on the porous Ti/SnO_2-Sb_2O_3-CNT/PbO_2 than that on the porous Ti/SnO_2-Sb_2O_3/PbO_2. About 95% and 87% of COD removal were achieved in 300 mins respectively. Hence, the organic compounds were more effectively degraded an oxidized on the porous Ti/SnO_2-Sb_2O_3-CNT/PbO_2. The high phenol removal rate can be ascribed to the larger active surface area[22]. In addition, the general current efficiency (GCE) and specific energy consumption (SEC) were also calculated, which were list in Table 3.

Obviously, all the above results indicate that CNT can effectively enhance the surface area of electrode, which improved the performance of the electrode. This agrees well with the experimental results presented above.

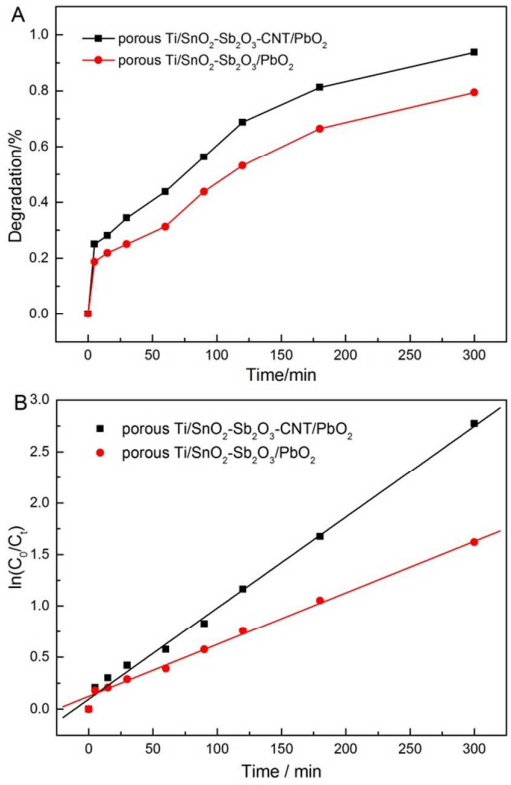

Fig.10 Phenol removal efficiency as a function of degradation time for different electrodes (A). Kinetic analysis of the curves (B). Operating condition: Na_2SO_4 concentration, 0.1mol L^{-1}; initial concentration, 100 mg L^{-1}; Current density: 30mA cm^{-2}; stirring rate: 800 r·min^{-1}.

Table 3 The General current efficiency (GCE) and Specific energy consumption (SEC) for different PbO_2 electrodes.

Electrode sample	GCE	SEC/kWh (kg COD)$^{-1}$
porous Ti/SnO_2-Sb_2O_3/PbO_2	61.3%	289.45
porous Ti/SnO_2-Sb_2O_3-CNT/PbO_2	67.1%	250.62

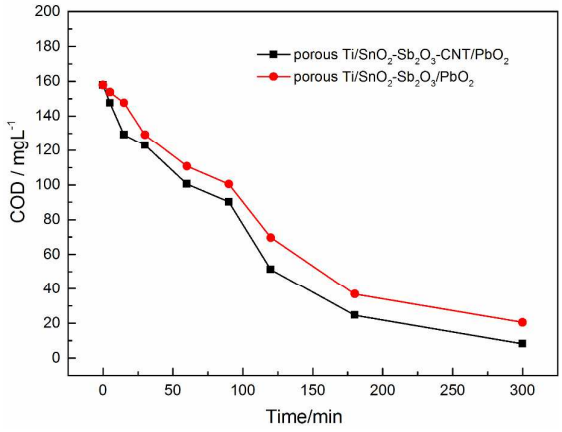

Fig.11 Variations of COD with electrolysis time for the different anodes in 80ml 100 mg/L phenol + 0.25mol/L Na_2SO_4 solution with current density of 30 mA/cm^2 at 25℃

3.3.2 Voltammetric characteristics of electrode. The two electrodes were characterized electrochemically by cyclic

voltammograms tests in a 0.5 mol L^{-1} Na_2SO_4 solution in the absence and in the presence of 100 mg L^{-1} phenol. The CV curves for the two electrodes were recorded between 0 V to 2.0 V (vs SCE) at a scan rate of 10 mV s^{-1}. As show in Fig.12, when 100 mg L^{-1}phenol was added to the supporting electrolyte, no additional peaks were found compared to the CV curve recorded in the reference solution, indicating that the direct electron transfer did not occur. Thus, it can be concluded that the phenol degradation in this system should be achieved via indirect electrochemical oxidation and mediated by hydroxyl radicals.

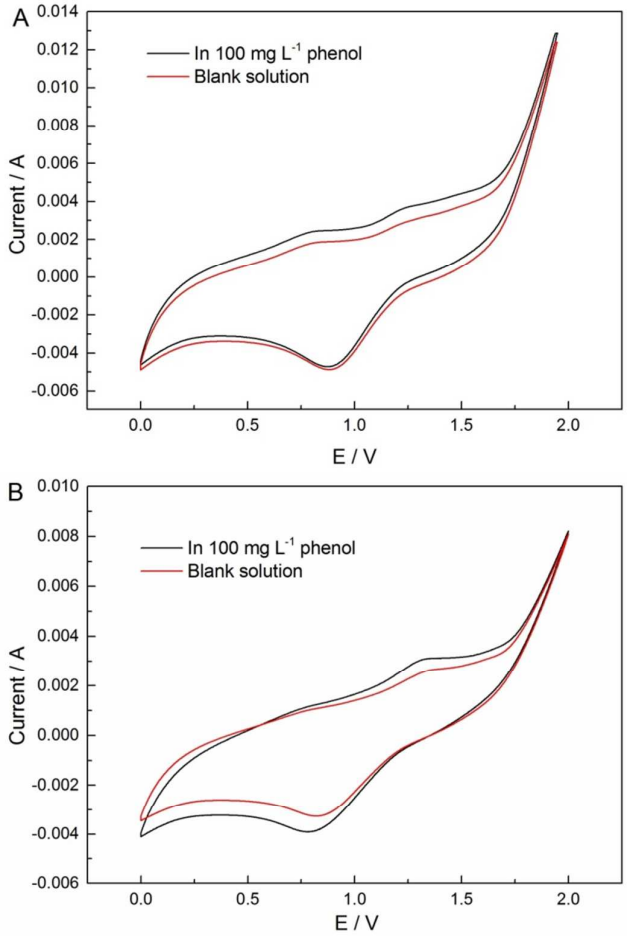

Fig.12 Cyclic voltammograms curves of different electrodes: (A) porous Ti/SnO_2-Sb_2O_3/PbO_2, (B) porous Ti/SnO_2-Sb_2O_3-CNT/PbO_2 in the absence and in the presence of phenol.

3.3.3. Hydroxyl radical (·OH) generation capacity of the electrodes. Generally, organic pollutants are mainly degraded by the indirect electrochemical oxidation mediated by ·OH radicals in the electro-catalytic oxidation process.[8, 41] Hence, quantitative determination of the generation ability of hydroxyl radicals in the electrochemical degradation process were necessary to be measured. During electrochemical treatment, terephthalic acid as a type of ·OH radical capture agent, can readily react with ·OH radicals to produce highly fluorescent product 2-hydroxyterephthalic acid. The amount of ·OH radicals formed was approximately equal to the amount of 2-hydroxyterephthalic acid, which was represented as a fluorescence intensity.[28] As can be seen in Fig.13, the fluorescence intensity of 2-hydroxyterephthalic acid around 425 nm for two electrodes increased with increasing the reaction time, indicating that ·OH radicals were indeed formed on the anodes and played an important role in electrochemical degradation test. Comparing the fluorescence intensity for the different electrodes at different reaction times, it was found that the fluorescence intensity for the porous Ti/SnO_2–Sb_2O_3-CNT/PbO_2 electrode was higher than that for the porous Ti/SnO_2–Sb_2O_3/PbO_2 electrode, which reveals the excellent electro-catalytic activity of the porous PbO_2 electrode. Therefore, the porous Ti/SnO_2–Sb_2O_3-CNT/PbO_2 electrode could oxidize pollutants more effectively compared with the porous Ti/SnO_2–Sb_2O_3/ PbO_2.

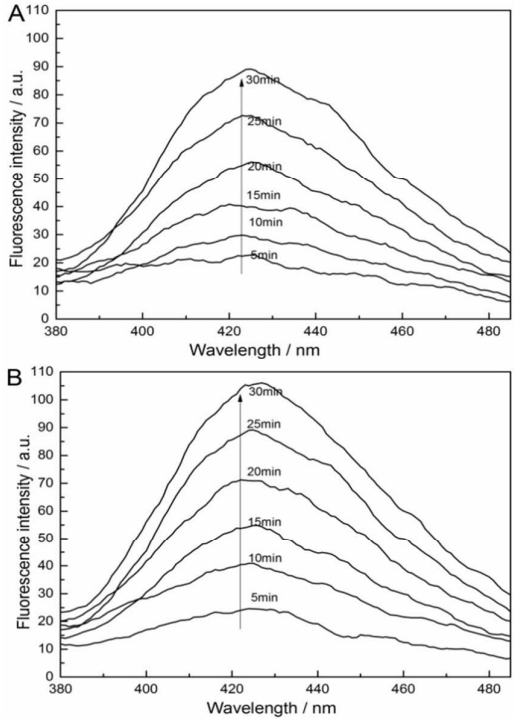

Fig.13 Fluorescence spectrum changes observed during the electro-catalytic oxidation process in a 0.5 mol L^{-1} aqueous solution of terephthalic acid using the prepared PbO_2: (A) porous Ti/SnO_2–Sb_2O_3/PbO_2 electrode, (B) porous Ti/SnO_2–Sb_2O_3-CNT/PbO_2 electrode.

4. Conclusions

A high effective porous Ti/SnO_2-Sb_2O_3-CNT/PbO_2 electrode was successfully prepared on a porous titanium substrate by thermal decomposition and electro-deposition method. The electrode modified with CNT versus without CNT has higher specific surface area, which can improve interlayer coating structure effectively and favors the formation of PbO_2 during electro-deposition. The voltammetric charge quantity indicated that the electrode modified with CNT enhanced the mass transfer rate on PbO_2 electrode. The results of accelerated life tests showed that the service life of porous Ti/SnO_2-Sb_2O_3-CNT/PbO_2 electrode was longer than that of electrodes without CNT-doped, which was 1.35 times that of porous Ti/SnO_2-Sb_2O_3/PbO_2. The electrode modified with CNT is then applied in phenol wastewater treatment and presents

excellent ability of organic pollutant oxidation and degradation compared with the electrode without CNT modification. After 5h,the phenol is almost completely decomposed using porous Ti/SnO_2-Sb_2O_3-CNT/PbO_2, and the COD removals reached 94.81%, while the values of porous Ti/SnO_2-Sb_2O_3/PbO_2 is just 87.01%. Besides, the general current efficiency (GCE) and specific energy consumption (SCE) were superior to that of the porous Ti/SnO_2-Sb_2O_3/PbO_2 (67.1%, 250.62 $kg^{-1}\cdot COD^{-1}$ versus 61.3%, 289.45 $kg^{-1}\cdot COD^{-1}$). In addition, CNT-doped can further increase the Hydroxyl radical (·OH) generation capacity. Considering the improved electro-catalytic oxidation performance and service life in practice, the porous Ti/SnO_2-Sb_2O_3-CNT/PbO_2 anodes can be prepared on a large scale and applied in industry.

Acknowledgements

The authors are grateful for the financial support provided by the Innovative Program of Activities for University in Shanghai (NO. PE2015029). Wenli Zhang (Jilin University) and Quansheng Zhang (Shanghai Institute of Technology) are also gratefully acknowledged for supplying experimental guidance and the electrochemical workstation, respectively.

References

1. H. Li, Y. Chen, Y. Zhang, W. Han, X. Sun, J. Li and L. Wang, *Journal of Electroanalytical Chemistry*, 2013, **689**, 193-200.
2. D. Shao, J. Liang, X. Cui, H. Xu and W. Yan, *Chemical Engineering Journal*, 2014, **244**, 288-295.
3. X. Duan, L. Tian, W. Liu and L. Chang, *Electrochimica Acta*, 2013, **94**, 192-197.
4. J. Niu, Y. Bao, Y. Li and Z. Chai, *Chemosphere*, 2013, **92**, 1571-1577.
5. J. Niu, H. Lin, J. Xu, H. Wu and Y. Li, *Environmental science & technology*, 2013, **47**, 4959-4959.
6. E. Brillas and C. A. Martínez-Huitle, *Applied Catalysis B: Environmental*, 2015, **166–167**, 603-643.
7. M. Panizza and G. Cerisola, *Chemical Reviews*, 2009, **109**, 6541-6569.
8. C. Martínez-Huitle and S. Ferro, *Chemical Society reviews*, 2006, **35**, 1324.
9. A. B. Velichenko, R. Amadelli, E. A. Baranova, D. V. Girenko and F. I. Danilov, *Journal of Electroanalytical Chemistry*, 2002, **527**, 56-64.
10. Y. Xia, Q. Dai and J. Chen, *Journal of Electroanalytical Chemistry*, 2015, **744**, 117-125.
11. G. Zhao, Y. Zhang, Y. Lei, B. Lv, J. Gao, Y. Zhang and D. Li, *Environmental science & technology*, 2010, **44**, 1754-1759.
12. Y. Shen, H. Xu, P. Xu, X. Wu, Y. Dong and L. Lu, *Electrochimica Acta*, 2014, **132**, 37-41.
13. L. Du, J. Wu and C. Hu, *Electrochimica Acta*, 2012, **68**, 69-73.
14. A. Fernandes, D. Santos, M. J. Pacheco, L. Ciríaco and A. Lopes, *Applied Catalysis B: Environmental*, 2014, **148–149**, 288-294.
15. L. Zhang, L. Xu, J. He and J. Zhang, *Electrochimica Acta*, 2014, **117**, 192-201.
16. J. P. Carr and N. A. Hampson, *Chemical Reviews*, 1972, **72**, 679-703.
17. M. Panizza, A. Kapalka and C. Comninellis, *Electrochimica Acta*, 2008, **53**, 2289-2295.
18. X. Hao, L. Jingjing, Y. Wei and W. Chu, *Rare Metal Materials and Engineering*, 2013, **42**, 885-890.
19. A. B. Velichenko and D. Devilliers, *Journal of Fluorine Chemistry*, 2007, **128**, 269-276.
20. Y. Feng, Y. Cui, B. Logan and Z. Liu, *Chemosphere*, 2008, **70**, 1629-1636.
21. Y. Feng, Y.-H. Cui, J. Liu and B. E. Logan, *Journal of hazardous materials*, 2010, **178**, 29-34.
22. H. Xu, A. Li and X. Cheng, *International Journal of Electrochemical Science*, 2011, **6**.
23. H. Lin, J. Niu, J. Xu, Y. Li and Y. Pan, *Electrochimica Acta*, 2013, **97**, 167-174.
24. R. Berenguer, C. Quijada and E. Morallón, *Electrochimica Acta*, 2009, **54**, 5230-5238.
25. A. Moncada, S. Piazza, C. Sunseri and R. Inguanta, *Journal of Power Sources*, 2015, **275**, 181-188.
26. Y. Song, G. Wei and R. Xiong, *Electrochimica Acta*, 2007, **52**, 7022-7027.
27. M. Manjaiah, S. Narendranath and S. Basavarajappa, *Transactions of Nonferrous Metals Society of China*, 2014, **24**, 12-21.
28. W. Zhao, J. Xing, D. Chen, Z. Bai and Y. Xia, *RSC Advances*, 2015, **5**, 26530-26539.
29. W. Zhang, H. Lin, H. Kong, H. Lu, Z. Yang and T. Liu, *International Journal of Hydrogen Energy*, 2014, **39**, 17153-17161.
30. S. Iijima, *nature*, 1991, **354**, 56-58.
31. F. Hu, Z. Dong, X. Cui and W. Chen, *Electrochimica Acta*, 2011, **56**, 1576-1580.
32. D. Yang, L. Zhu and X. Jiang, *Journal of Electroanalytical Chemistry*, 2010, **640**, 17-22.
33. F. Hu, X. Cui and W. Chen, *Electrochemical and Solid-State Letters*, 2010, **13**, F20.
34. X. Duan, F. Ma, Z. Yuan, L. Chang and X. Jin, *Journal of Electroanalytical Chemistry*, 2012, **677-680**, 90-100.
35. W. Zhao, J. Xing, D. Chen, Z. Bai and Y. Xia, *RSC Advances*, 2015.
36. H. Vogt, *Electrochimica acta*, 1994, **39**, 1981-1983.
37. S. Trasatti, *Electrochimica acta*, 1991, **36**, 1659-1667.
38. Y. Chen, L. Hong, H. Xue, W. Han, L. Wang, X. Sun and J. Li, *Journal of Electroanalytical Chemistry*, 2010, **648**, 119-127.
39. D. Pavlov, A. Kirchev, M. Stoycheva and B. Monahov, *Journal of Power Sources*, 2004, **137**, 288-308.
40. J. Zhao, C. Zhu, J. Lu, C. Hu, S. Peng and T. Chen, *Electrochimica Acta*, 2014, **118**, 169-175.
41. X. Zhu, J. Ni, H. Li, Y. Jiang, X. Xing and A. G. L. Borthwick, *Electrochimica Acta*, 2010, **55**, 5569-5575.